Particle Acceleration with High-Intensity Lasers

Report
by
Christian Homann

Lund Reports on Atomic Physics, LRAP-376
Lund, March 2007

Contents

Chapter 1

Introduction

The availability of lasers that reach peak intensities above 10^{18} W/cm^2 has opened up an entirely new field of non-linear optics, the so-called "relativistic regime". At these intensities electrons are accelerated to relativistic velocities in the laser field, which leads to a number of new non-linear effects including for example relativistic focusing, wakefield generation and multiple harmonic generation. One of the key phenomena is the occurrence of strong longitudinal field effects. These originate in the Lorentz force

$$\vec{F} = e(\vec{E} + \vec{v} \times \vec{B}) \tag{1.1}$$

where, contrary to linear and "weak" non-linear optics, the $\vec{v} \times \vec{B}$-term can no longer be neglected, leading to a complicated motion of the electron in the laser field. A natural unit in this context is $a_0 = \frac{eA}{m_e c}$ (A is the electromagnetic vector potential) representing the quivering momentum of the electron, normalized to $m_e c$. The longitudinal displacement of the electron due to the $\vec{v} \times \vec{B}$-term scales with a_0^2, whereas the transverse displacement due to the electric field is proportional to a_0. That means for $a_0 > 1$ the interaction with the magnetic field even plays the dominating role ($a_0 = 1$ corresponds to an intensity $I \approx 2 \cdot 10^{18}$ W/cm^2 for $\lambda = 800$ nm). When focusing a laser to these intensities on for example a thin metal foil, these longitudinal forces will lead to a charge separation in the foil, which can be used for proton and heavy ion acceleration (to be described in more detail later). When focusing into a gas even more forces as for example the ponderomotive force come into play and can lead to very efficient electron acceleration (also described in more detail later).
During my MAXLAS short term training in Lund, I had the great opportunity to get a first glimpse into this new exciting field of physics. I took part in two experiments related to electron acceleration (Chapter 3) and one experiment in proton acceleration (Chapter 4). But first a breif overview of the Lund Laser System.

Chapter 2

The Multi-Terawatt Laser System in Lund

2.1 Overview of the Lund Laser System

The very high peak intensities needed to access the relativistic regime (see Introduction) have only been made possible by the rapid development of lasers in the last 20 years (see figure 2.1). A key step to higher laser intensities was

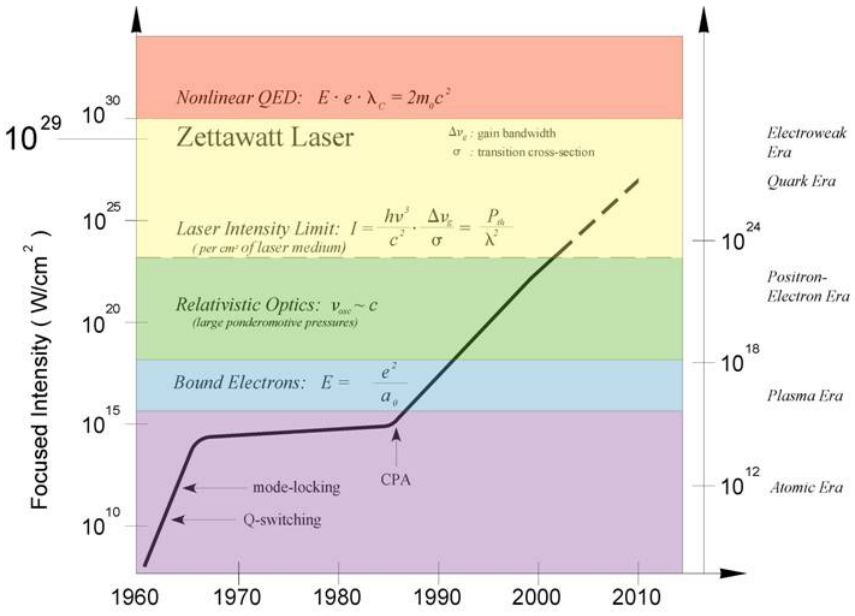

Figure 2.1: Evolution of the laser energy since 1960

the invention of "chirped pulse amplification" (CPA) in 1985 by Strickland and

Mourou [1] . At that time the laser peak intensity had not increased significantly for about 20 years. A further increase seemed not possible because of non-linear effects in the amplification medium, which lead to a destruction of the wavefront and spectrum of the pulse and ultimately also of the amplifying medium. CPA overcame this problem by stretching the seed pulse in time before it is amplified, therefore lowering the intensity in the amplifying media and minimizing nonlinear effects. After the amplification the pulse is compressed back to its original duration (figure 2.2). The Lund Laser System as well as most other laser systems nowadays that reach peak intensities above 10^{18} W/cm^2 are based on the CPA technique.

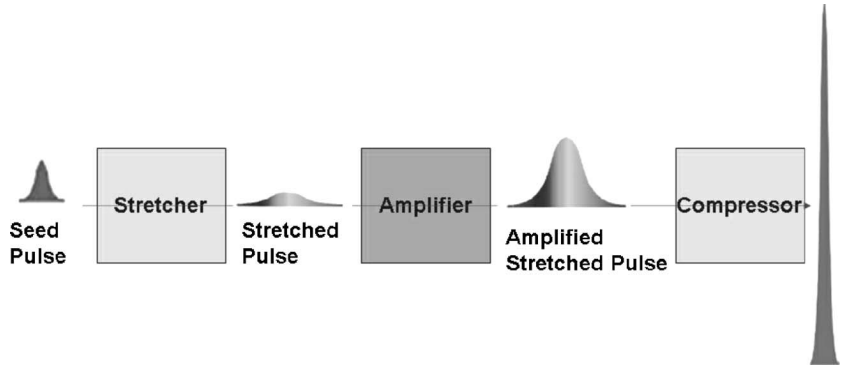

Figure 2.2: Principle of chirped pulse amplification (CPA)

A schematic of the Lund Laser is shown in figure 2.3. It is an ultra-short pulse laser with titanium sapphire as broadband amplifying medium. It delivers output pulses with an energy of 1.5 J and duration of 35 fs to 45 fs (depending on the operation mode) at a repetition rate of 10 Hz.

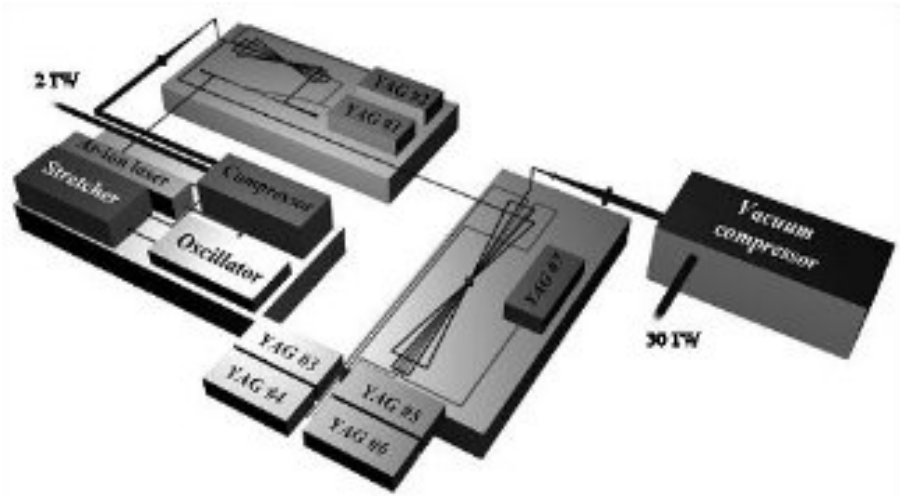

Figure 2.3: Schematic of the Multi-Terawatt Laser System in Lund [2]

The oscillator is seeded by 3.8 W of cw-light at 532 nm and produces pulses with an energy of 5 nJ, a duration of 20 fs and a central wavelength of 800 nm with a repetition rate of 80 MHz. These pulses then pass through an acousto-optical device (called "Dazzler") that can shape their spectrum (spectral phase and amplitude) to a certain extent. After the Dazzler the pulses are either immediately stretched to about 350 ps in a setup of mirrors and gratings or are first amplified in the "pre-amplifier" (the operation and influence of the pre-amplifier will be discussed in section 2.2). It can be easily switched between the setting without and with pre-amplifier by flipping a switchable mirror. After the stretcher one out of 8 million pulses is injected into a regenerative amplifier (regen), giving the final repetition rate of 10 Hz. In the regen the pulse gets amplified to approximately 5 mJ. The Ti:sapphire crystal in the regen is pumped by 65 mJ from a pulsed Nd:YAG-laser, delivering 12 ns pulses at a center wavelength of 532 nm. The regen output is then further amplified in a 5-pass butterfly setup, pumped by 1.2 J of Nd:YAG energy. After this stage the laser pulses have an energy of approximately 300 mJ. They are split into two pulses of 200 mJ and 100 mJ energy. The higher energy pulse is directly sent to a compressor and into one of the target areas. This beamline with a peak power of approximately 2 TW is the "low-intensity arm" of the Lund Multi-Terawatt Laser System. The lower energy pulse gets spatially filtered and is sent to an additional 4-pass butterfly amplifier, where it gets boosted to a total energy of 1.5 J. The key optic in this final amplifier is a cryogenically cooled 19 mm thick Ti:sapphire crystal, pumped with a total energy of 6 J per pulse by five Nd:YAG-lasers.
Already before entering the final amplifier the beam is expanded by a telescope from its original 8 mm to 16 mm to avoid damaging of the crystal. After the amplifier the beam is further expanded by a second telescope to a diameter of 50 mm. This is necessary to avoid damaging of the following compressor gratings and all optics thereafter. The compressor gratings are located in vacuum ($\lesssim 10^{-4}$ mbar), because the compressed pulses would self-focus when propagating in air under normal pressure. The compressor has a transmission efficiency of 60% so that the final pulses have approximately 900 mJ in a duration of 35 fs. This beamline is the "high-intensity arm" of the Multi-Terawatt Laser System in Lund. The peak power is about 35 TW.

2.2 Laser Contrast and the Pre-Amplifier

A very important parameter for high-intensity laser systems, besides pulse energy and duration, is the laser temporal contrast on a ns and ps time scale. It is defined as the ratio between the peak pulse intensity and the intensity level some ns / some 100 ps before the peak. The two main reasons for this prepulse energy are amplified spontaneous emission (ASE) originating mainly from the regen, and incomplete compression due to high-order effects and spectral clipping. The ASE produces a several nanosecond long pedestal, which at the Lund Laser is cut to approximately one nanosecond duration by the use of a fast Pockels cell. As shown in figure 2.4 the level of the ASE strongly depends on the seed energy into the regen.
A self-evident idea to improve the contrast is therefore to increase the seed energy into the regen. It is however important that the seed pulses are as "clean"

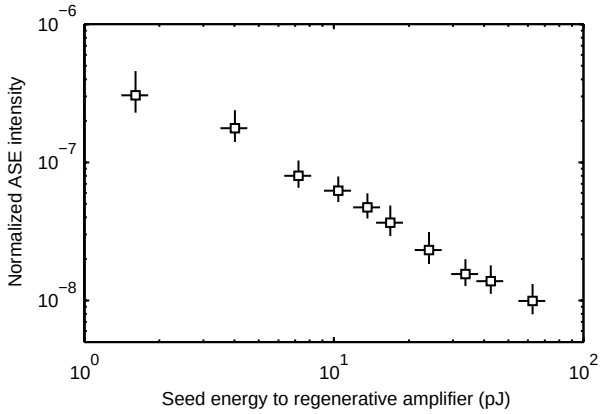

Figure 2.4: When the seed energy into the regen is increased the ASE level decreases

as possible, meaning they should have as small a pedestal as possible. This idea was put into practice by Martin Glimtoft as his master project by building an additional amplifier, the pre-amplifier, between the oscillator and the strecher [3]. Although completed in January 2006, the pre-amplifier was not put to use until December 2006. During my stay here it was optimized and made ready for a routinely application. The setup is shown in figure 2.5.
It consists of a 4-pass amplifier followed by a saturable absorber. The 12 mm long Ti:sapphire crystal is pumped longitudinally from both sides by a frequency doubled Nd:YAG laser (Quantel, Brilliant 10). The pump power can be adjusted with a $\lambda/2$-plate followed by a thin film polarizer located directly after the YAG. The pulses are then split by a 50:50 beam splitter and sent into the crystal. We found a pump energy of 42 mJ per pulse in one arm and 48 mJ in the other arm to be well suited for a stable operation of the pre-amplifier. With these settings the most amplified oscillator pulses get amplified by a factor of about 13000. After the four passes the pulses are focused by a lens (focal length 200 mm) and recollimated by a lens with a focal length of 102 mm. Between these two lenses the saturable absorber (Schott RG850, 2 mm) is placed. This is the optic used for cleaning the pulses. It's normal transmission for light with a wavelength of 800 nm is about 10^{-3}. However at high fluences the filter bleaches and the transmission gets much higher. Schott RG 850 is a colloidally coloured glass containing cristallites of a certain species. These absorb visible light and therefore account for the low transmittance in this wavelength region. At high fluences all cristallites in the illuminated region go into an excited state and therefore do not absorb visible photons any more. For the incoming laser pulses that means that the relatively low-intensity pedestal before the main pulse is attenuated very strongly, the high-intensity part of the pulse however is transmitted quite well. The filter should be placed as close to the focus as possible to give the highest transmittence and therefore the highest seed energy into the regen. In our case that meant a distance of 230 mm from the focusing lens. Was the filter placed closer to the focus, a plasma was created on its surface, reducing the transmittance. With these settings a transmission of 64% was achieved,

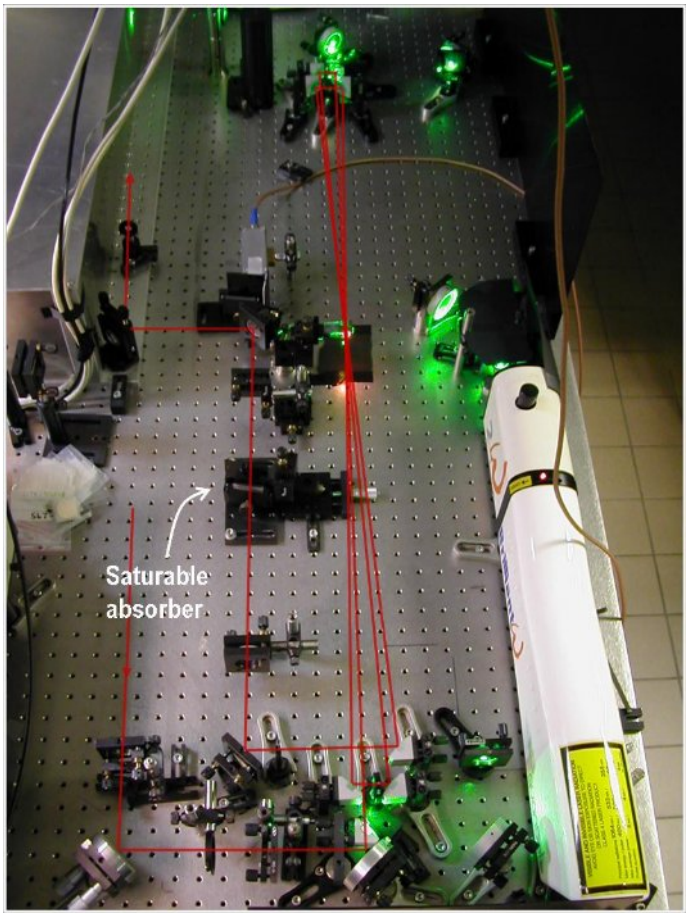

Figure 2.5: Picture of the pre-amplifier

giving a total gain of the pre-amplifier setup of around 8000.
To reach the same regen output energy with this increased seed, two possibilties exist. One alternative is to reduce the number of roundtrips in the regen cavity, the other is to reduce the pump energy. We have tested both possibilities and found that a combination of both is most advantageous. When the number of roundtrips is reduced from 15 to 13 and the pump energy is reduced so that the output energy of the regen stays constant, we measured a contrast of 10^9. Taking away 2 more roundtrips and increasing the pump power produces approximately the same contrast, removing even more roundtrips leads to a worse contrast ratio. Increasing the number of roundtrips above 13 and reducing the pump power even more reduces the output power of the regen drastically and saturation is no longer reached in the next amplifier. The best achieved contrast ratio with the setup was around $1.7 \cdot 10^9$, in which case however the output after the first butterfly amplifier was about 10% less than usual. A contrast ratio of 10^9 was achieved routinely, but also with slightly less output power after the first butterfly amplifier compared to operation without pre-amplifier.
The drawback of using the pre-amplifier is that it narrows the spectral bandwith

of the pulses. This leads to a longer pulse duration after compression. It increases from about 35 fs without pre-amplifier to about 45 fs with pre-amplifier.

Chapter 3

Electron acceleration

3.1 Theory

As already mentioned in the introduction, laser pulses at relavistic intensities interact in an interesting new way with matter. Not only gets the exposed medium instantanously ionized, but the electrons experience strong longitudinal forces due to the $\vec{v}\times\vec{B}$-term and the ponderomotive force, which leads to electron acceleration in the laser forward direction. Even stronger acceleration in this direction can be achieved, when a plasma wave is created that the electrons can "surf".
Given an initially uniform, collision-free plasma with cold electrons, it can be shown that when the electrons are displaced from the equilibrium position they will start to oscillate with a frequency

$$\omega_{\mathrm{P}} = \sqrt{\frac{n_{\mathrm{e}} e^2}{m_{\mathrm{e}} \varepsilon_0}} \tag{3.1}$$

(assumed that the positive ions are so heavy that they do not move at all). ω_P is called the (electron) plasma frequency and n_e is the electron density. Plasma waves of this kind are also known as "Langmuir waves". They can be excited by different mechanisms, for example by an electron beam coming from an accelerator [4] or by a beating wave of two co-propagating laser pulses with frequencies ω_1 and ω_2 so that $\omega_1 - \omega_2 = \omega_{\mathrm{P}}$ [5]. Short high-intensity laser pulses even allow the creation of plasma waves with only one laser pulse. If the pulse duration is of the order of the plasma period, then the pulse can excite a plasma wave in its wake which travels nearly at the speed of light.
But only creating a plasma wave is not sufficient to achieve acceleration of electrons to high energies. If one considers for example an electron that is initially at rest, it will first get accelerated by the plasma wave in one direction, but as it starts to move, the plasma wave will overtake the electron and accelerate it in the opposite direction, and so forth. That means an electron originally at rest will stay approximately at rest. Only electrons that move already in the beginning almost with the phase velocity of the plasma wave, stay long enough

in one accelerating structure of the wave to gain high energies. But once injected into such an accelerating structure, the electrons can gain a lot of energy due to the extremely strong electric fields there (of the order of 1 to 10 GV/m). The occurence of these huge acceleration gradients (compared to 50 MV/m in conventional accelerators) make this acceleration scheme (called "laser wakefield acceleration" (LWFA)) so interesting.
In LWFA one distinguishes between the linear (or moderately non-linear) regime and the strongly non-linear regime. In the linear regime the plasma wave (i.e. the elecron density in the laser direction) has a sinusoidal form with an amplitude that scales linearly with the intensity of the laser pulse. The non-linear regime instead is characterised by a more "peaked" structure in the electron density (still periodic) and the proportionality of amplitude and laser intesity is no longer valid. In the non-linear regime higher acceleration gradients can be achieved, whereas the linear regime allows a better control of the properties of the accelerating structure and so hopefully of the accelerated beam. Another advantage of the linear regime is that it can be reached with relatively low electron densities (around 10^{16}-10^{17} cm^{-3} for laser intensities about 10^{19} W/cm^2), whereas the non-linear regime requires much higher electron densities (around 10^{18}-10^{19} cm^{-3}). This means that the dephasing length, which is defined as the maximum distance an electron can travel within the plasma wave until it reaches its maximum energy, being proportional to $n_e^{-3/2}$, is longer in the linear regime. If one achieves to keep the electron within the plasma wave for the whole dephasing length, this also means that in the linear regime very high electron energies (several GeV) should be possible.
Both approaches are currently being investigated by several groups in the world. I had the great opportunity to take part in two experiments, each of them related to one approach.

3.2 Studying the properties of a plasma wave in the linear regime within a capillary tube

3.2.1 Objective of the experiment

As just explained, LWFA in the linear regime is one possible approach to achieve strong electron acceleration, because of the potentially long electron dephasing length. The main problem nowadays is to keep the laser pulse focused over this whole length (which can reach tens of centimetres). This is necessary because for todays lasers only the focused beam is intense enough to efficiently drive the plasma wave. Possibilities to do so include using plasma channels [6] to guide the laser pulse and capillary tubes as waveguides.
We tried to investigate the latter approach. The main objective of our experiment was to analyse the amplitude of the plasma wave created in a dielectric capillary tube by looking at the spectrum modifications of a probe beam. The corresponding theory is described in detail in [7]. The idea is, that a plasma wave having a sinusoidally electron density in the propagation direction also has a refractive index distribution of that kind. That means that different parts of a long probe beam (long compared to the wavelength of the plasma wave), that

is co-propagating with the plasma wave, experience different refractive indices. Therefore they move with slightly diffferent velocities, which leads to spectral modulations within the probe beam (see figure 3.1).

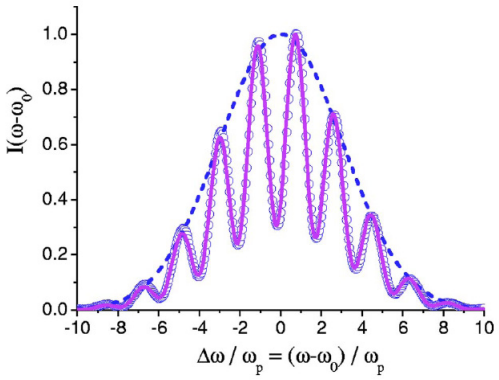

Figure 3.1: Analytical (solid line) and numerical (dots) prediction of the spectrum of the probe laser pulse after propagation in a capillary over a of 4 cm, and initial spectrum at the capillary entrance (dashed line) [7]

3.2.2 Setup

A schematic of the setup used is shown in figure 3.2. The main beam (800 nm, 700 mJ, 35 fs) and the blue beam (400 nm, 5 mJ, 300 ps) are overlapped on a dichroic mirror and focused with a 1.5 m focal length - parabola (f/30 for the main beam) onto the entrance of a capillary tube. We had capillary tubes made of glass with an internal diameter of 100 μm and various lengths of 6, 7 and 8 cm. Each capillary had two small slits approximately 5 mm away from its ends that were used to inject hydrogen gas at various pressures. The exit plane of the capillary was imaged onto various diagnostics (2 CCD cameras to look onto the spatial mode of the main respectively the probe beam and 2 spectrometers to record their spectra).

Until the end of the campaign unfortunately none of the diagnostics produced very valuable data. The main reason for this was probably the poor coupling of the main beam to the guiding mode of the capillary. To achieve an optimal coupling, the spot size of the laser beam and the diameter of the guiding structure must be matched. This implies strong requirements for the pointing stability of the laser beam. Even as small fluctuations in position as half the spot size can lead to a destruction of the entrance of the glass capillary. Although a very good pointing stability of the laser beam could be achieved through several actions (for example switching off the cryogenic cooler for the last amplifier crystal during the shots), the rather extreme requirements for this experiment could not be fulfilled. This led to a very quick degeneration of the coupling efficency over only a few shots per capillary.
The second main problem of this experiment was the not known distribution of

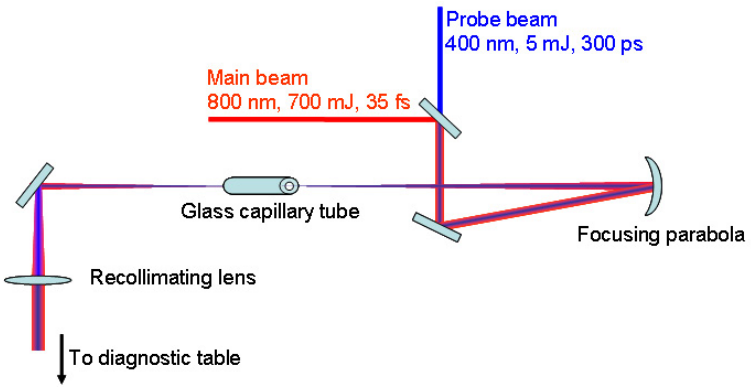

Figure 3.2: Schematic of the setup

the gas density inside the capillary at a given injection gas pressure. Therefore a parametric scan of the injection gas pressure would have been necessary to find settings where a plasma wave is excited. This was not possible with the very limited number of good shots (high coupling efficiency) we had.

3.3 Electron acceleration in the bubble regime and undulator radiation

3.3.1 Objective of the experiment

In the second experiment on electron acceleration I took part in, we were trying to reach the highly non-linear wakefield regime. In this regime new phenomena as for example wave-breaking can occur. In a 1D geometry this happens when the the amplitude of the motion of the electrons is larger than the plasma wavelength. Wave-breaking leads to self-injection of electrons into the plasma wave, which then get accelerated. Recently it has been shown that when certain conditions are fullfilled (concerning laser energy, focal spot diameter, pulse length and electron density), this mechanism can lead to a plasma "bubble" [8] (see figure 3.3) and to quasi monoenergetic eletron beams [9][10][11].

The main objective of the experiment was to send this electron bunch through an undulator and thus create undulator radiation in the VUV range. The use of laser-plasma based electron beams for generating undulator radition is currently of great scientific interest because of the unique properties of the electron bunches. Due to their temporal shortness ($<$30 fs) and their small divergence their emittance is much lower than for electron beams from conventional accelerators. The undulator radiation will therefore be much more brilliant than previously possible.

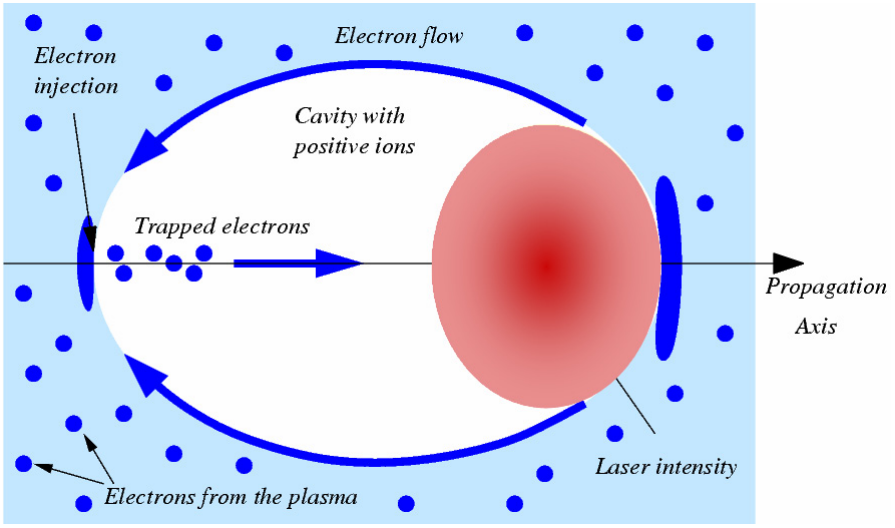

Figure 3.3: If certain conditions are fullfilled than the laser pulse expells efficiently electrons from the plasma radially (mainly due to the ponderomotive force). Thus a cavity free from electrons forms behind the laser, which is surrounded by a dense region of electrons. Behind the bubble, electronic trajectories intersect each other and a few electrons are injected into the cavity. These electrons get accelerated along the laser axis and form a quasi monoenergetic electron beam. [12]

3.3.2 Setup

A very simplified schematic of the setup used is shown in figure 3.4. The main beam (800 nm, 800 mJ, 35 fs) is focused with a f/10 off-axis parabola (focal length 450 mm) onto a supersonic gas jet. The gas jet is pulsed and provides an atomic density n_a of the order of 10^{19} cm^{-3}. As helium is used as gas this means an electron density n_e of $2 \cdot n_\mathrm{a}$ when the gas is fully ionized by the laser. For a stable and most energetic electron beam it is important that the' laser is focused onto the middle of the front side of the gas jet (diameter 2 mm) just below the nozzle. To ensure that the gas jet was motorized so that it was moveable under vacuum in all three directions.

At the beginning of the experiment a Lanex screen was placed after the gas jet instead of the undulator. Lanex is a scintillating material that emits green light when hit by fast electrons. By looking at it with a CCD camera (shielded with color filters that transmit only in this wavelength region) we could optimize the spatial profile of the electron beam. Adjustable parameters to do so were the position of the gas jet, the electron density (via the the gas pressure) and the pulse duration of the laser beam (by translating one of the gratings in the compressor). To measure the energy of the accelerated electrons we inserted a pair of magnets in front of the Lanex screen, which produced a uniform magnetic field of 0.7 Tesla. The magnetic field deflected the electrons as a function of their energy and therefore acted as a spectrometer. An evaluation of the position of

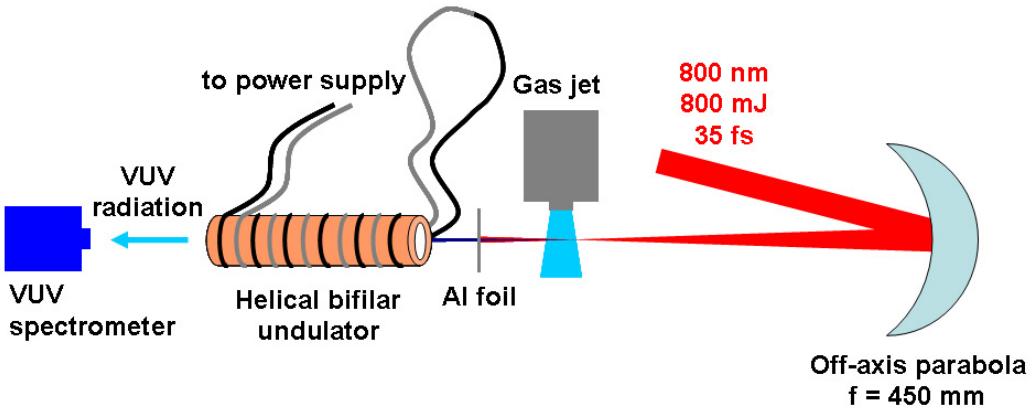

Figure 3.4: Schematic of the setup used

the electrons hitting the Lanex screen thus gives a measure of their energy. Besides the just described detectors some more diagnostics were installed. Among them an imaging system to look at the Thompson scattered light from the plasma channel, a forward imaging system to look at the laser mode and the spectrum after the gas and an interferometric line to look at density perturbations within the gas due to the plasma channel. Since all these diagnostics were hardly used during the time I took part in the experiment they are not described in more detail here.

3.3.3 Results

When this report was written, the experimantal campaign was still going on. At that time we managed to produce a stable electron beam that contained electrons with energies up to about 90 MeV. We were able to send the electron beam through the undulator but we could not yet observe undulator radiation.

Chapter 4

Proton acceleration

The second main topic I worked on during my time in Lund is laser-driven proton acceleration. This field, together with laser-driven heavy-ion acceleration, is currently attracting significant scientific interest because of its interesting potential future applications. Among these are for example proton therapy for cancer treatment, the production of short living isotopes for positron emission tomography, and ignitors in laser-driven inertial fusion. Especially for the medical applications particle accelerators based on lasers could provide great benefits due to their small size and low cost compared to conventional acceleration techniques.

4.1 Theory

In contrast to electron acceleration where the laser is focused into a gas, the target in proton acceleration is a thin (of the order of 10 μm) metal foil. The incident laser pulse drives electrons through the metal foil, which form a Debye sheath at the rear surface of the target. Inside this sheath exist extremely strong electric fields (of the order of TV/m) which lead to ionization of contaminants (for example H_2O) on the surface. The positively charged ions (mainly protons) are accelerated in the electric field normal to the target surface and escape together with hot electrons in a quasi-neutral cloud [13]. With this acceleration mechanism, called target normal sheath acceleration (TNSA, see figure 4.1), proton energies up to 58 MeV have been achieved [14].

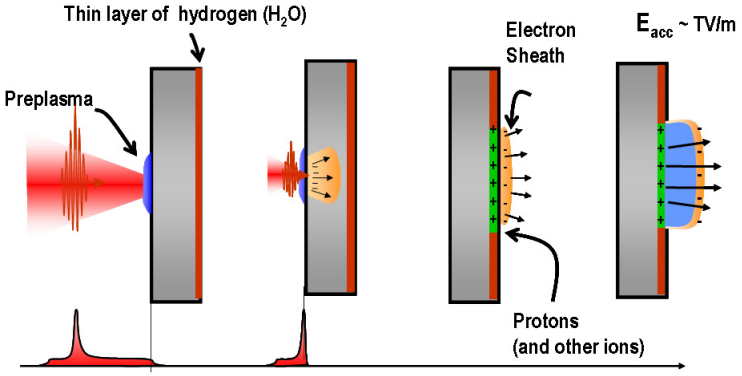

Figure 4.1: Target normal sheath acceleration of protons

4.2 Active beam control in laser-driven proton acceleration

To match the requirements for applications (as mentioned before), even higher proton energies and a better control of the proton beam are necessary. One important parameter in this respect is the divergence of the proton beam. In previous experiments it has been shown that the divergence can be influenced by shaping the rear surface of the target [15]. Focusing of the proton beam has been achieved by a micro-machined spherically shaped target. As these targets are difficult to produce, therefore very expensive, and not very flexible in respect of changing their properties, optically shaped targets would be very attractive. In our experiment we tried to go a first step in this direction and to optically steer the proton beam in a well defined direction. In a previous experiment here in Lund, a steering of the proton beam away from the original target normal and towards the laser forward direction was observed [16]. This was attributed to a shock wave driven through the foil by the ASE pedestal of the laser pulse. When the shock wave reached the rear surface it bent the foil, leading to a locally new target normal.
In our recent experiment, we now tried to keep the ASE as low as possible, and to use a second well controlled laser pulse to drive a shock in the foil (see fig. 4.2). The objective was to have full control over the strength and position of the shock wave to steer the proton beam to our wishes. For this purpose a low-intensity frequency doubled Nd:YAG-laser pulse was focused to a line onto the target. Depending on the relative position and timing of the YAG- and the main laser pulse as well as the energy of the YAG-pulse a steering of the proton beam could indeed be observed.

4.2.1 Setup

To have the lowest possible ASE, i.e. the best contrast, the pre-amplifier described in section 2.2 was used in this experiment. In figure 4.3 a typical result

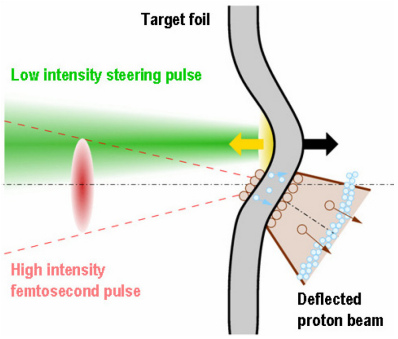

Figure 4.2: A low-intensity beam (green) is used to heat and ablate the front side of the target. The heated plasma expands into the vacuum and exerts a very high pressure on the target. This causes a shock wave travelling through the target and bending the rear surface locally. Therefore protons which are accelerated according to TNSA by the high intensity laser pulse are deflected compared to the case without low intensity beam.

of our daily contrast measurements is shown. With this contrast ratio of 10^9 it was possible to use aluminium foils as thin as 3 μm as target (and probably even thinner foils would have been possible).

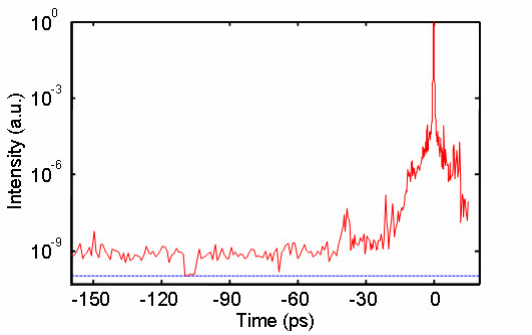

Figure 4.3: Measured contrast with a third-order autocorrelator (red) and the noise level when the beam is blocked (blue)

A schematic of the experimental setup is shown in 4.4. The main beam was focused with a f/3 off-axis parabola (focal length 150 mm) to a spot with a full width at half maximum of 3.3 μm. Containing an energy per pulse of about 600 mJ and a measured pulse duration τ_0 of 45 fs this means a peak intensity of

$$I = 2\left(\frac{ln2}{\pi}\right)^{3/2}\frac{E}{\tau_0 x_{FWHM}^2} = 2.5\cdot 10^{19}\ \mathrm{W/cm^2} \tag{4.1}$$

The mirror before the parabola and the parabola itself were motorized and a CCD camera was used to look through a microscope (magnification of 40) at the focal plane. That made it possible to correct for almost all abberations in

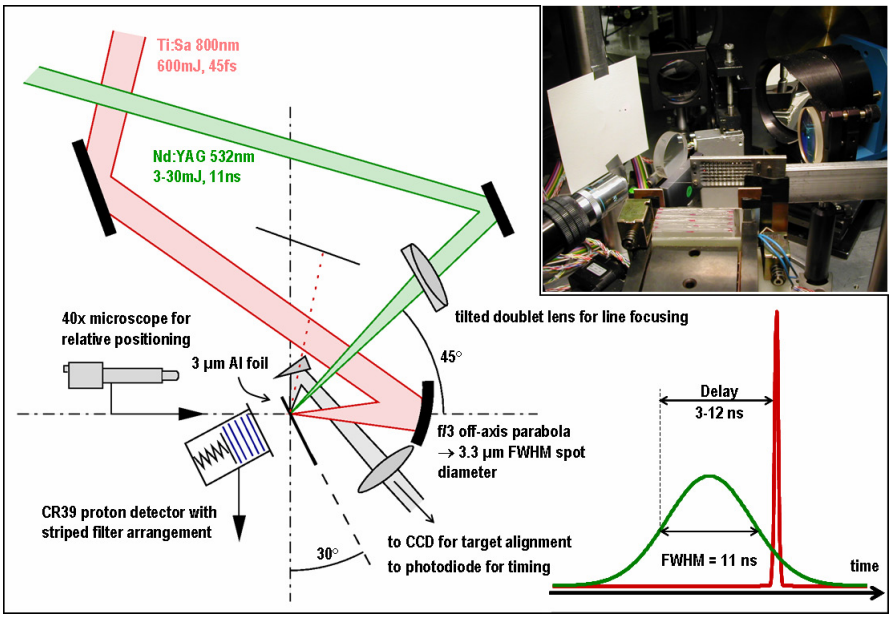

Figure 4.4: Schematic of the setup used (left) and photograph of the target and the surrounding optics and detectors (upper right). The sketch in the lower right corner shows our definition of the time delay of the two pulses.

the beam (for example astigmatism) and to get this nearly diffraction limited spot. The microscope was also motorized to be able to move it out of the focal plane and to move in the target mount instead. The 3 μm thin aluminium foil was clamped in a metallic frame, which could be moved under vacuum in all three spatial directions. To place the target exactly in the focal plane we set up an imaging system that imaged the front side of the target onto a CCD at the outside of the chamber. When illuminating the target with a HeNe laser we could make sure that the specular reflection was always imaged sharply onte the same spot on the CCD, which meant that the target then was always in the same plane. With this technique we also could ensure that the target was not tilted vertically. To avoid back reflection of the laser beam into the laser system, the target was not perpendicular to the laser axis, but tilted by approximately 30° (see fig. 4.4).
The pulse for creating the shock wave (in the following called "steering beam") was provided by the oscillator of a Nd:YAG laser. It contained a maximal energy of about 30 mJ at a center wavelength of 532 nm and had a duration of 11 ns. It was focused with a 200 mm focal length doublet lens. To get a line focus the lens was tilted by approximately 10°, introducing strong astigmatism. The lens was then positioned in such a way that the target was in the focal plane for one direction, producing a horizontal line focus in the target plane of about 200 μm x 20 μm size. To be able to adjust the relative position of the main and the steering beam the lens was motorized in the two directions perpendicular to the laser propagation direction. When instead of the aluminium target a scattering foil (in our case a white fiber grinding foil) was moved into the focal plane,

we were able to see both the main and the steering beam with our front side imaging system at the same time. This enabled us to position the two beams with an accuracy of about 2 μm. Together with the pointing instabilities of the beams and a slow drift of the lens motor between shots, the accuracy of the relative position measurement was 4 μm.
To measure the time delay between the two beams we split off a small fraction of the light in the imaging line with a glass plate and sent it onto a fast photodiode. With an oscilloscope we could in that way determine the time delay with an accuracy of better than 1 ns. For a definition of the time delay see the sketch at the bottom right of figure 4.4.
As proton detector we used 5 cm x 5 cm big and 1 mm thick CR39 plates. CR39 is a special plastic that is insensitive to fast electrons and X-ray radiation, but sensitive to protons. The protons produce small damages in the plastic, and when etching with a 85°C hot sodium hydroxide solution (NaOH, mass percentage 20%, i.e. for example 800 mg water and 200 mg NaOH) for about 30 minutes small pits (one for each proton) appear that can be counted with a microscope. A stack of 20 CR39 plates was mounted parallel to the target at a distance of 30 mm (in some cases 56 mm). With a tricky mechanic a new piece of CR39 could be placed at the front of the stack for each shot. In front of the first plate a striped filter arrangement (see figure 4.5) was placed. Each layer

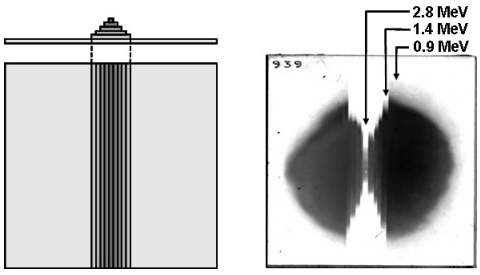

Figure 4.5: Filter arrangement in front of the CR39 detector (left) and typical developed CR39 sample (right)

of the filter arrangement consisted of a 13 μm thick aluminium foil. The filters shielded the CR39 from low energy protons (E $<$ 0.9 MeV) and enabled us to detect the spatial distribution of protons with different kinetic energies on every shot.

4.2.2 Results

To study the properties of the shock and especially the influence it has on the proton beam we made parametric scans of the relative position and timing of the two beams and of the energy contained in the steering beam.
First we scanned the vertical position of the horizontal line focus at a fixed time delay of 7.5 ns and energy of the steering beam of 29 mJ (corresponding to a peak intensity of 40 GW/cm^2). 15 μm from the overlapping position we observe significant proton beam steering upwards when the line focus is below the main

beam, and downwards when it is above. Noteworthy is that the proton beam is steered as a whole, that means all energies are deflected by the same angle. 30 μm from the overlap we see no effects of the steering beam on the proton emission. At the overlap position itself a strong defocusing in the vertical direction and a disappearing of high energy protons (E > 1.4 MeV) is observed (see fig. 4.6).

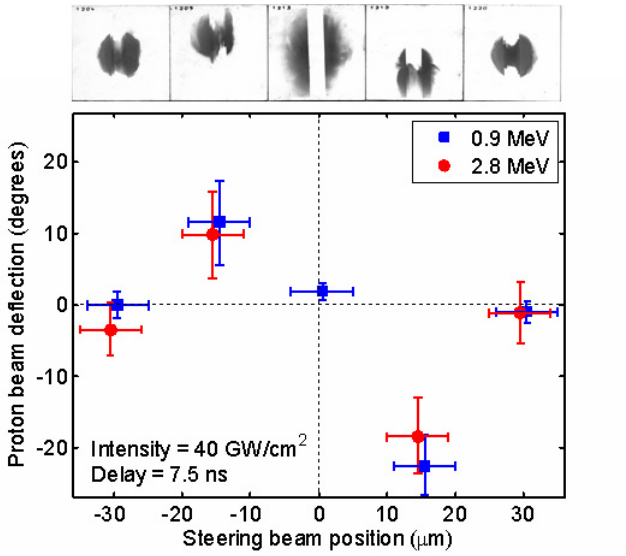

Figure 4.6: For a fixed time delay and fixed intensity of the Nd:YAG-beam a clear dependence of the deflection angle of the relative position can be seen. The error bars in position correspond to the 4 μm explained in the text, in angular deflection they show the standard deviation calculated from 3 shots per data point (at the overlap position only one good shot was observed, hence the error bars are missing).

These observations agree very well with the intuitive picture of figure 4.2. They also impose restrictions on the lateral dimension of the shock (being smaller than 30 μm under these conditions) and suggest that the diameter of the proton source is also smaller than 30 μm.
Second, when we changed the arrival time of the steering beam, at a position 15 μm below the main beam, we see that the proton deflection angle increases for longer delays (fig. 4.7). At the longest delay of 12 ns, the high energy protons disappear. This again can be easily understood in our simple model. The more time the shock has to act, the more will the rear surface of the target foil be bent and therefore the more will the proton beam be deflected. At the very long time delay of 12 ns the rear surface itself gets probably ionized leading to weaker electric fields in the Debye sheath and hence to a disappearence of the higher energy protons.
Third, when we positioned the line focus 10 μm above the proton source, we observe an increasing proton beam deflection for increasing steering pulse intensity (fig. 4.8). And again, at the highest intensity (40 GW/cm^2) the most energetic protons are gone.

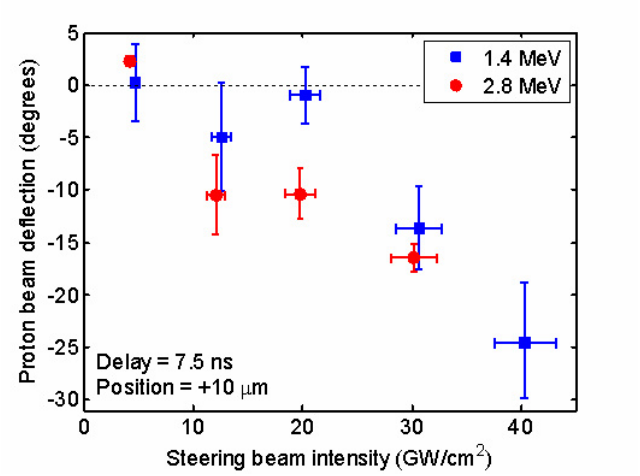

Figure 4.7: For a fixed relative position and time delay the deflection angle increases with increasing energy

We think this is due to the fact that the induced ablation pressure grows with laser intensity. Therefore the shock in the target is stronger, increasing the magnitude of the local deformation. At the highest steering beam intensity the structure of the rear surface probably starts to fell apart.

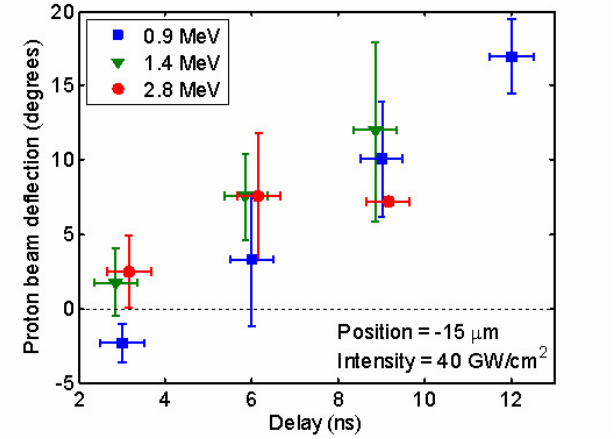

Figure 4.8: For a fixed relative position and energy the deflection angle increases with increasing time delay

4.2.3 Conclusion and Outlook

In conlusion, all our observations agree very well with the picture of TNSA in combination with a deformed rear surface by a laser-driven shock wave. The next step would be to focus the proton beam with this mechanism. One could for example think of producing a ring focus, which should form a crater-shaped rear surface. When the diameter of this valley is chosen correctly this should act similar to the micro-machined targets used in [15].
In the last few days of the experimental campaign we split the steering beam into two beams with slightly different directions by using a birefringent wedge. This produced two lines in the focal plane that were separated by approximately 40 μm. According to our model this should lead to a focusing of the proton beam in one direction. This was not observed. To get a better understanding of the process we placed a mesh (280 lines per inch) 0.5 mm behind the target. We then sometimes detected a deformation of the mesh pattern on the images, but the deformation was always symmetrical. This suggests that we succeded to move the virtual source of the protons, but not in the way our model predicts. Further analysis of the existing data and probably a new experimental campaign where parametric scans (for example in the line seperation distance) are made will be necessary to get a real understanding of the process.

Acknowledgements

This last half a year was a very enjoyable and instructive time for me. Although work was sometimes quite intense, I always enjoyed what I was doing and I learned a lot of things. The person who contributed most to this was my supervisor Claes-Göran Wahlström. He always took his time for me, explained me everything I asked and helped me wherever he could, be it within the institute or off the job. Thank you very very much!
But of course there were also many other people who made the time I spent in Lund so good. I want to thank especially my two group colleagues Olle Lundh and Yannick Glinec who were always open for all my questions, tried to involve me as a newby in this field as much as possible in all the experiments and with whom I always had fun in- and outside the lab. Special thanks also to Anders Persson, Emilie Pourtal, Marko Swoboda, Minna Ramkull, Henrik Steen and Bertil Hermansson for their kindness and help.
Since the group I was working in is strongly involved in many European-access campaigns, I had the great opportunity to work with many different people from all over Europe. This was very exciting and stimulating for me and I learned many things from them. Thanks to Enrico Brunetti, Brigitte Cros, Dino Jaroszynski, David Patin, Richard Shanks, Gregory Vieux and Franck Wojda ("capillary experiment"), Christos Kamperidis, Stefan Kneip, Zulfikar Najmudin and Stuart Mangles ("undulator experiment") and David Carrol, David Neely and Paul McKenna ("protons").
Finally I want to thank Anne L'Huilliere who as the coordinator of the MAXLAS project in Lund made this stay possible for me. I am very glad that I had the oppurtunity to be here!

Bibliography

[1] A.D. Strickland and G. Mourou, Opt. Commun. **56**, 212 (1985)

[2] J. Mauritsson, PhD Thesis, LRAP-312, Lund University (2003)

[3] M. Glimtoft, Master Thesis, LRAP-352, Lund University (2006)

[4] M.J. Hogen, C.D. Barnes, C.E. Clayton, F.J. Decker, S. Deng, P. Emma, C. Huang, R.H. Iverson, D.K. Johnson, C. Joshi, T. Katsouleas, P. Krejcik, W. Lu, K.A. Marsh, W.B. Mori, P. Muggli, C.L. OŠConnell, E. Oz, R.H. Siemann, and D. Walz, Phys. Rev. Lett. **95**, 054802 (2005)

[5] C.E. Clayton, M.J. Everett, A. Lal, D. Gordon, K.A. Marsh, and C. Joshi, Phys. Plasmas **1** 1753 (1994)

[6] A. Butler, D.J. Spence, and S.M. Hooker, Phys. Rev. Lett. **89**, 185003 (2002)

[7] N.E. Andreev, M.V. Chegotov, B. Cros, P.Mora, and G. Vieux, Phys. Plasmas **13**, 053109 (2006)

[8] A. Pukhov and J. Meyer-ter-Vehn, Appl. Phys. B **74**, 355 (2002)

[9] S. P. D. Mangles, C. D. Murphy, Z. Najmudin, A. G. R. Thomas, J. L. Collier, A. E. Dangor, E. J. Divall, P. S. Foster, J. G. Gallacher, C. J. Hooker, D. A. Jaroszynski, A. J. Langley, W. B. Mori, P. A. Norreys, F. S. Tsung, R. Viskup, B. R. Walton, and K. Krushelnick, Nature **431**, 535 (2004)

[10] C. G. R. Geddes, Cs. Toth, J. van Tilborg, E. Esarey, C. B. Schroeder, D. Bruhwiler, C. Nieter, J. Cary, and W. P. Leemans, Nature **431**, 538 (2004)

[11] J. Faure, Y. Glinec, A. Pukhov, S. Kiselev, S. Gordienko, E. Lefebvre, J.-P. Rousseau, F. Burgy, and V. Malka **431**, 541 (2004)

[12] Y. Glinec, PhD Thesis, Ecole Polytechnique, Paris (2006)

[13] S. C. Wilks, A. B. Langdon, T. E. Cowan, M. Roth, M. Singh, S. Hatchett, M. H. Key, D. Pennington, A. MacKinnon, and R. A. Snavely, Phys. Plasmas **8**, 542 (2001)

[14] R. A. Snavely, M. H. Key, S. P. Hatchett, T. E. Cowan, M. Roth, T. W. Phillips, M. A. Stoyer, E. A. Henry, T. C. Sangster, M. S. Singh, S. C. Wilks, A. MacKinnon, A. Offenberger, D. M. Pennington, K. Yasuike, A. B. Langdon, B. F. Lasinski, J. Johnson, M. D. Perry, and E. M. Campbell, Phys Rev. Lett **85**, 2945 (2000)

[15] P. K. Patel, A. J. Mackinnon, M. H. Key, T. E. Cowan, M. E. Foord, M. Allen, D. F. Price, H. Ruhl, P. T. Springer, and R. Stephens, Phys. Rev. Lett. **91**, 125004 (2003)

[16] F. Lindau, O. Lundh, A. Persson, P. McKenna, K. Osvay, D. Batani, and C.-G. Wahlström, Phys. Rev. Lett. **95**, 175002 (2005)